Inorganic Chemistry

Article

pubs.acs.org/IC

Probing the Copper(II) Binding Features of Angiogenin. Similarities and Differences between a N-Terminus Peptide Fragment and the Recombinant Human Protein

Diego La Mendola,[†] Daniel Farkas,[‡] Francesco Bellia,[§,∥] Antonio Magrì,[†] Alessio Travaglia,[§,⊥] Örjan Hansson,[‡] and Enrico Rizzarelli*[,§]

[†]Istituto di Biostrutture e Bioimmagini-CNR-Catania, Viale A. Doria 6, 95125 Catania, Italy

[‡]Department of Chemistry, University of Gothenburg, PO Box 462, SE-40530 Gothenburg, Sweden

[§]Dipartimento di Scienze Chimiche, Università di Catania, Viale A. Doria 6, 95125 Catania, Italy

Supporting Information

ABSTRACT: The angiogenin protein (hAng) is a potent angiogenic factor and its cellular activities may be affected by copper ions even if it is yet unknown how this metal ion is able to produce this effect. Among the different regions of hAng potentially able to bind copper ions, the N-terminal domain appears to be an ideal candidate. Copper(II) complexes of the peptide fragments encompassing the amino acid residues 4−17 of hAng protein were characterized by potentiometric, UV−vis, CD, and EPR spectroscopic methods. The results show that these fragments have an unusual copper(II) binding ability. At physiological pH, the prevailing complex species formed by the peptide encompassing the protein sequence 4−17 is [CuHL], in which the metal ion is bound to two imidazole and two deprotonated amide nitrogen atoms disposed in a planar equatorial arrangement. Preliminary spectroscopic (UV−vis, CD, and EPR) data obtained on the copper(II) complexes formed by the whole recombinant hAng protein, show a great similarity with those obtained for the N-terminal peptide fragments. These findings indicate that within the N-terminal domain there is one of the preferred copper(II) ions anchoring site of the whole recombinant hAng protein.

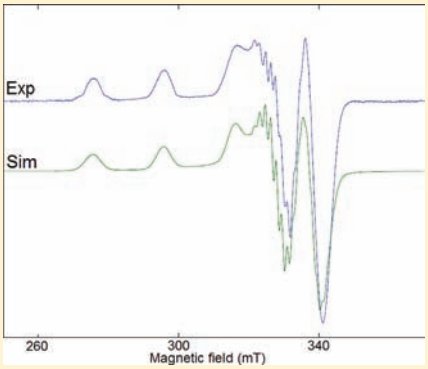

INTRODUCTION

Human angiogenin (hAng), a 14-kDa member of the ribonuclease (RNase) superfamily, is a single-chain blood plasma protein present in physiological conditions.[1−3] hAng is one of the most potent angiogenic factors in vivo, being active on the chicken chorioallantoic membrane up to fractions of nanogram.[1] High serum levels of hAng characterize patients affected by different types of cancers, suggesting a strictly correlation with tumor growth, progression and even severity.[1,4] The presence of hAng is required for cell proliferation induced by other angiogenic agents such as basic fibroblast growth factor (bFGF) and vascular endothelial growth factor (VEGF).[5] However, angiogenesis is a complex multistep process in which new blood capillaries grow from pre-existing vessels[6] and the precise molecular mechanism by which hAng affects these processes is not yet clear.[7] It is known that hAng binds to membrane proteins and undergoes nuclear translocation, inducing a wide range of cellular responses in endothelial and smooth muscle cells.[7−9] Three distinct regions of the protein seem to be necessary for the angiogenic activity: the catalytic site for RNase activity involving residues His-13, Lys-40 and His-114, the putative cell binding region encompassing residues 60−68 (KNGNPHREN) and the nuclear translocation sequence 31−35 (RRRGL).[8,9]

Interestingly, the binding affinity between hAng and endothelial cells is largely increased in the presence of copper ions.[10] It is well-known that copper(II) ions perform a strong angiogenic signal in vivo, but the specific molecular mechanism by which it works and the targets of its activity remain unclear.[11] It is also well-known that serum Cu^{2+} levels are raised in a wide variety of human cancers, including breast, prostate, colon, lung and brain cancers, and they are related to the tumor severity.[12,13] Recently, it has been demonstrated that extracellular translocation of the cytosolic copper occurs during angiogenesis processes in vitro, therefore suggesting that the metal coordination by an extracellular protein involved in angiogenesis, such as hAng and/or VEGF, could play an important role.[14]

It has been shown that hAng tightly binds about 2.4 copper ions per molecule at physiological pH, by means of atomic absorption spectroscopic and immobilized metal ion affinity chromatographic techniques.[15] The copper(II) ions binding to the protein increased its interaction with endothelial cells and then its angiogenic activity.[15] On the contrary, it has been hypothesized that copper(II) and hAng are both angiogenic factors, but that they act through different biological pathways.

Received: June 16, 2011
Published: December 7, 2011

Chart 1. Schematic View of the Primary Sequence of hAng(4−17), hAng(4−9), and hAng(10−17)

hAng(4-17) = Ac-**SRYTHFLTQHYDAK-NH$_2$**

hAng(4-9) = Ac-**SRYTHF-NH$_2$**

hAng(10-17) = Ac-**LTQHYDAK-NH$_2$**

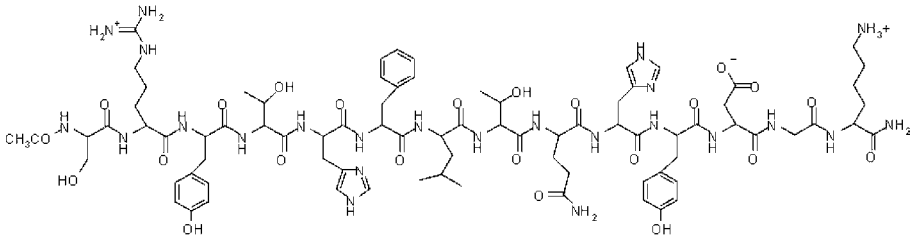

hAng(4-17)

As far as we know, there are no detailed molecular studies on copper(II) ions interaction with hAng.[16]

To elucidate the binding sites within the hAng, we are currently studying the interaction of Cu^{2+} with different peptide fragments belonging to the protein. Copper(II) complexes with the peptide encompassing the putative endothelial cell binding domain of hAng, Ac-KNGNPHREN-NH$_2$, have been characterized; [Cu(Ac-KNGNPHREN-NH$_2$)H$_{-2}$] is the main species in the physiological pH range, showing a 3N1O equatorial coordination mode in a square based pyramidal stereochemistry.[17] Within the different regions of hAng potentially able to bind copper ions, the N-terminal domain which includes the first α helix domain (α-H1 residues 5−13) appears to be an ideal candidate. As a matter of fact, this region is solvent exposed and contains two histidine residues (His-8 and His-13),[18−20] which are generally elective anchoring sites for copper(II) ions.

In this work, we report the synthesis of the peptide fragment hAng(4−17) (Ac-SRYTHFLTQHYDAK-NH$_2$) encompassing the hAng N-terminal domain, blocked at the N- and C-termini by acetylation and amidation, respectively (Chart 1); the copper(II) complex species were characterized by means of a combined potentiometric and spectroscopic (EPR, CD, UV−vis) study. The peptide fragments hAng(4−9) (Ac-SRYTHF-NH$_2$) and hAng(10−17) (Ac-LTQHYDAK-NH$_2$) (see Chart 1) were also studied to determine the involvement of the single histidine residues, His-8 and His-13, in copper(II) complex species. Furthermore, the copper(II) binding features with the hAng peptide fragments here studied results to be useful to probe the coordination features of the whole recombinant hAng protein. For this purpose, the recombinant hAng protein was expressed and a preliminary characterization of its copper(II) complexes was performed by means of EPR, CD and UV−vis measurements.

EXPERIMENTAL SECTION

Materials. All *N*-fluorenylmethoxycarbonyl (Fmoc)-protected amino-acids, and 2-(1-*H*-benzotriazole-1-yl)-1,1,3,3-tetramethyluronium tetrafluoroborate (TBTU), were obtained from Novabiochem (Switzerland); Fmoc-PAL-PEG resin, *N*,*N*-diisopropyl-ethylamine (DIEA), *N*,*N*-dimethylformamide (DMF, peptide synthesis grade) and 20% piperidine-DMF solution were from Applied Biosystems; *N*-hydroxybenzotriazole (HOBT), triisopropylsilane (TIS), trifluoroacetic acid (TFA), 3-morpholinopropane-1-sulfonicacid (MOPS) were purchased from Sigma/Aldrich. All the other chemicals were of the highest available grade and were used without further purification.

Peptide Synthesis and Purification. The peptides Ac-SRYTHFLTQHYDAK-NH$_2$ hAng(4−17), Ac-SRYTHF-NH$_2$ hAng(4−9) and Ac-LTQHYDAK-NH$_2$ hAng(10−17) were synthesized in the N-acetylated and C-amidated form to avoid end-group effects and to mimic more properly their character of a protein internal fragment. They were assembled using the solid phase peptide synthesis strategy on a Pioneer Peptide Synthesizer. All amino acid residues were added according to the TBTU/HOBT/DIEA activation method for Fmoc chemistry on Fmoc-PAL-PEG resin (loading 0.22 mmol/g, 0.33 mmol scale synthesis, 1.5 g of resin). Other experimental details have already been reported.[21]

The peptides were purified by means of a preparative reversed-phase high-performance liquid chromatography (rp-HPLC). Purification was performed on a Varian PrepStar 200 model SD-1 chromatography system equipped with a Prostar photodiode array detector with detection at 222 nm. The peptide was eluted with solvent A (0.1% TFA in water) and B (0.1% TFA in acetonitrile) on a Vydac C$_{18}$ 250 × 22 mm (300 Å pore size, 10−15 μm particle size) column, at a flow rate of 10 mL/min. Analytical rp-HPLC analyses were performed using a Waters 1525 instrument, equipped with a Waters 2996 photodiode array detector with detection at 222 nm.

The peptide samples were analyzed using gradient elution with solvent A and B on a Vydac C$_{18}$ 250 × 4.6 mm (300 Å pore size, 5 μm particle size) column, at a flow rate of 1 mL/min.

The peptides hAng(4−9) and hAng(10−17) were eluted according to the following protocol: from 0 to 5 min isocratic gradient in 0% B, then linear gradient from 0 to 25% B over 15 min, finally isocratic gradient in 25%B from 20 to 30 min.

The peptide hAng(4−17) was eluted according to the following protocol: from 0 to 5 min isocratic gradient in 0% B, then linear gradient from 0 to 25% B over 20 min, finally isocratic gradient in 25% B from 25 to 35 min.

The peptides were characterized by means of electron spray ionization mass spectrometry (ESI-MS).

Ac-SRYTHF-NH$_2$ (hAng(4−9)). [R_t = 21.30 min]. Calculated mass for $C_{39}H_{54}N_{12}O_{10}$ M = 850.93, ESI-MS [Obsd m/z: $(M + H)^+$ 851.8; $(M + 2H)^{2+}$ 426.5].

Ac-LTQHYDAK-NH$_2$ (hAng(10−17)). [R_t = 22.40 min]. Calculated mass for $C_{45}H_{69}N_{13}O_{14}$ M = 1016.12, ESI-MS [Obsd m/z: $(M + H)^+$ 1017.2; $(M + 2H)^{2+}$ 509.1].

Ac-SRYTHFLTQHYDAK-NH$_2$ (hAng(4−17)). [R_t = 26.50 min]. Calculated mass for $C_{82}H_{118}N_{24}O_{23}$ M = 1807.98, ESI-MS [Obsd m/z: $(M + H)^+$ 1809.1; $(M + 2H)^{2+}$ 906.2; $(M + 3H)^{3+}$ 603.9].

Protein Expression and Purification. A codon-optimized gene for hAng inserted into the pET22b expression vector was purchased from Sloning BioTechnology and successfully transformed into the *E. coli* expression host BL21. Expression of recombinant hAng was

dx.doi.org/10.1021/ic201300e | *Inorg. Chem.* 2012, 51, 128−141

carried out following a previously reported method.[22] The protein was refolded from inclusion bodies according to the procedure developed by Jang et al.[23] The BCA method (Pierce) was used to determine the total protein content when setting up the optimum refolding conditions. The purification of recombinant hAng was performed using an automated chromatographic workstation (Akta prime, GE Healthcare). The procedure consisted of two chromatographic steps. A cation-exchange purification was carried out by using a 15 × 1.6 cm column packed with SP Sepharose Fast Flow (GE Healthcare). After a washing step with 25 mM Tris-HCl and 0.2 M NaCl (pH 8.0), the recombinant protein was eluted with 25 mM Tris-HCl and 0.8 M NaCl (pH 8.0). The fractions containing hAng were pooled, concentrated and further purified by gel-filtration chromatography. A prepacked Hiprep 26/60 Sephacryl S100 column equilibrated with 25 mM Tris and 150 mM NaCl (pH 8.0) was used to maintain a good separation at a flow rate of 1 mL/min. The purity of the protein was evaluated by means of SDS-PAGE (Criterion XT 10% bis-Tris) and the ribonucleolytic activity was determined as previously described.[24] The concentration of hAng was determined using ε_{280} = 12 500 M^{-1} cm^{-1}.[15]

Ribonucleolytic Activity. The ribonucleolytic activity of the protein toward tRNA has been determined by measuring the formation of perchloric acid-soluble fragments as reported in literature,[22,24] with few modifications. Briefly, the recombinant protein (0.5 μM) and tRNA (2 mg/mL) were incubated with different equivalents of $Cu(NO_3)_2$ (0−50 μM) at pH 7.4 (33 mM MOPS, 33 mM NaCl). After 2 h at 37 °C, the solution (300 μL) was diluted with ice-cold $HClO_4$ 3.4% (700 μL) and kept on ice for 10 min. Finally, the sample was centrifuged (10 000 × g) for 10 min and the absorbance of perchloric acid soluble fragments was measured at 260 nm.

Potentiometric Titrations. Potentiometric titrations were performed with two home-assembled fully automated apparatus sets (Metrohm E654 pH-meter, combined micro pH glass electrode, Orion 9103SC, Hamilton digital dispenser, Model 665) controlled by the appropriate software set up in our laboratory. The titration cell (2.5 mL) was thermostatted at 298.0 ± 0.2 K, and all solutions were kept under an atmosphere of argon, which was bubbled through a solution having the same ionic strength and temperature as the measuring cell. KOH solutions (0.1 M) were added through a Hamilton buret equipped with 1 cm^3 syringes. The ionic strength of all solutions was adjusted to 0.10 M (KNO_3). To determine the stability constants, solutions of the ligands (protonation constants) or the ligands with Cu^{2+} (copper complex constants) were titrated by using 0.1 M sodium hydroxide. The ligand concentration ranged from 2.4 to 4.0 × 10^{-3} and from 3.4 to 4.2 × 10^{-3} M for the protonation and complexation experiments, respectively. A minimum of three independent runs were performed to determine the protonation constants, while four independent experiments were run for the copper(II) complexation constants.

Metal to ligand ratios between 2:1 and 1:1, were employed. The initial pH was always adjusted to 2.4. To avoid systematic errors and verify reproducibility, the EMF values of each experiment were taken at different time intervals. Other details were as previously reported.[25] To obtain protonation and complexation constants, the potentiometric data were refined using Hyperquad,[26] which minimizes the error square sum of the measured electrode potentials through a nonlinear iterative refinement of the sum of the squared residuals, U, and also allows for the simultaneous refinement of data from different titrations:

$$U = \Sigma(E_{exp} - E_{calc})^2$$

where E_{exp} and E_{calc} are the experimental and calculated electrode potentials, respectively. Errors in stability constant values are reported as three times standard deviations.

The formation reaction equilibria of ligands with protons and copper(II) ions are given in eq 1:

$$pCu + qH + rL = Cu_pH_qL_r \quad (1)$$

in which L are the peptides under study. The stability constant β_{pqr} is defined in eq 2:

$$\beta_{pqr} = [Cu_pH_qL_r]/[Cu]^p.\ [H]^q.\ [L]^r \quad (2)$$

The species distribution as a function of the pH was obtained by using the computer program Hyss.[27]

Spectroscopic Studies. *UV−vis Measurements.* UV−vis spectra were recorded at 25 °C, by using an Agilent 8453 or a Varian Cary 500 spectrophotometer. The concentrations of the peptides and copper(II) used to record absorption spectra were the same as those for the potentiometric titrations. Combined spectroscopic and potentiometric metal-complex titrations were performed into a 3 mL quartz cuvette with a 1 cm path length to get the spectrum in the visible region at each pH value simultaneously. These experiments were replicated at least three times for each copper-peptide system. Spectroscopic data were processed by using the HYPERQUAD program.[26]

CD Measurements. CD spectra were obtained at 25 °C under a constant flow of nitrogen on a Jasco model 810 spectropolarimeter at a scan rate of 50 nm min^{-1} and a resolution of 0.1 nm. The path lengths were 1 or 0.1 cm, in the 190−800 nm range. The spectra were recorded as an average of 10 or 20 scans. Calibration of the instrument was performed with a 0.06% solution of ammonium camphorsulfonate in water. The CD spectra of the copper(II) complexes on varying the solution pH were obtained in both the 200−400 and 300−800 nm wavelength regions. All the solutions were freshly prepared using double distilled water. The copper(II) ion and peptide concentrations used for the acquisition of the CD spectra in the visible region were identical to those used in the potentiometric titrations. Far UV CD spectra were acquired by using copper(II) ion and peptide concentrations ranging from 5.0 × 10^{-6} to 1.0 × 10^{-5} M. The results are reported as ε (molar adsorption coefficient) and $\Delta\varepsilon$ (molar dichroic coefficient) in M^{-1} cm^{-1}.

hAng protein samples were diluted to a final concentration of 10 μM in 10 mM MOPS (pH = 7.4) in the presence or absence of 1 mol equiv of Cu^{2+}.

EPR Measurements. A Bruker Elexsys E500 CW-EPR spectrometer driven by a PC running XEpr program under Linux and equipped with a Super-X microwave bridge, operating at 9.3−9.5 GHz, and a SHQE cavity was used throughout this work. All EPR spectra of frozen solutions of copper(II) complexes were recorded at 150 K by means of a ER4131VT variable temperature apparatus. EPR magnetic parameters were obtained directly from the experimental EPR spectra, always calculating them from the second and the third line to get rid of second-order effects. Instrumental settings of EPR spectra recordings of the copper(II)-peptide complexes were as follow: number of scans 1−5; microwave frequency 9.344−9.376 GHz; modulation frequency 100 kHz; modulation amplitude 0.2−0.6 mT; time constant 164−327 ms; sweep time 2.8 min; microwave power 20−40 mW; receiver gain 1 × 10^4-2 × 10^5. Copper(II) complexes were prepared by addition of the appropriate amount of isotopically pure copper, taken from a $^{63}Cu(NO_3)_2$ 0.05 M solution, to the peptide solution. The preparation of the complex solutions involved metal-to-ligand ratios which were 1:1 and 2:1. Copper(II) complexes solutions were prepared in 10% methanol−water mixture. EPR spectra of the recombinant hAng protein were acquired at a protein concentration of 0.5 mM in 25 mM MOPS and 150 mM NaCl (pH 7.4) and in the presence of 1 mol equiv of Cu^{2+}. The experimental parameters were: microwave frequency, 9,434 GHz; microwave power, 20 mW; modulation amplitude, 0.2 mT. hAng protein samples were diluted to a final concentration of 10 μM in 10 mM MOPS (pH = 7.4) in the presence of 1 mol equiv of Cu^{2+}.

Simulations of EPR spectra were performed with Matlab (MathWorks) using the EasySpin toolbox (version 3.1.0).[28]

RESULTS AND DISCUSSION

Proton and Copper(II) Complexes with hAng(4−17), hAng(4−9), and hAng(10−17) Affect the Conformation

dx.doi.org/10.1021/ic201300e | Inorg. Chem. 2012, 51, 128−141

Features of the hAng Peptide Fragments. Protonation constants of the three peptides (Chart 1) were determined by potentiometric titrations (Table 1); as expected in the investigated pH range, hAng(4−9) and hAng(10−17) has two and four protonation sites, respectively. In hAng(4−9), the Tyr-6 group shows the highest p*K* value, while the other protonation constant is referred to the imidazole nitrogen of the His-8 residue. The carboxylate and the imidazole groups of hAng(10−17) show p*K* values similar to those reported in the literature;[29,30] the overlap of the p*K* values pertinent to the dissociation of Tyr-14 and protonation of Lys-17 does not allow to unambiguously assign single p*K* values, though the literature data indicate that the ε-amino group of lysine shows generally a higher p*K* value than the tyrosine hydroxyl group.[31]

Table 1. Protonation Constants (log β_{pqr}) and p*K* Values for hAng(4−9), hAng(10−17), and hAng(4−17) (T = 298 K, I = 0.1 M KNO_3)[a]

species	hAng(4−9)	hAng(10−17)	hAng(4−17)
HL	9.97 (2)	10.72 (1)	10.82 (1)
H_2L	16.42 (3)	21.08 (1)	20.42 (1)
H_3L		27.76 (1)	29.17 (1)
H_4L		31.90 (2)	35.94 (2)
H_5L			41.96 (2)
H_6L			45.70 (2)
p*K* COO^-		4.14	3.74
p*K* His	6.45		6.02
p*K* His		6.67	6.77
p*K* Tyr	9.97		8.75
p*K* Tyr		10.36	9.60
p*K* Lys		10.72	10.82

[a]Standard deviations (3σ values) are given in parentheses.

The fragment hAng(4−17) contains six protonation sites. The lowest p*K* value belongs to the protonation equilibrium of the carboxylate group, in agreement with that reported for other peptides containing an aspartic residue.[29,30] The protonation of the two histidyl residues takes place in an overlapping process. The average value for the protonation of the imidazole nitrogens (p*K* = 6.39) is very close to that of other histidine containing peptides but lower than that obtained for hAng(10−17).[31,32] The protonation processes of Tyr-6, Tyr-14, and Lys-17 also take place in an overlapping equilibrium, thus each protonation constant value should be considered as a macroconstant. The presence of different networks of side-chain interactions could be the origin of some differences in the p*K* values among the investigated peptides.

Far-UV CD spectra of hAng(4−17), hAng(4−9), and hAng(10−17) were obtained in the pH range 4−10 (Figure 1S). The presence of a band with a minimum at 196 nm and a band with a maximum at 228 nm suggest a prevalent random coil conformation of the three peptides, in the pH range 4−6. Increasing the pH value, the peptide hAng(4−17) displays a slight decrease of the intensity of the bands centered at 196 nm and at 228 nm, in a similar way to that reported for other peptide systems.[33] Above pH 7, the histidine residues are deprotonated and the spectra show an increase of the band at 196 nm, and the appearance of two new bands displaying a maximum at 213 and a minimum at 224 nm. These effects are more evident at pH 10, and a broad band centered at 245 nm is

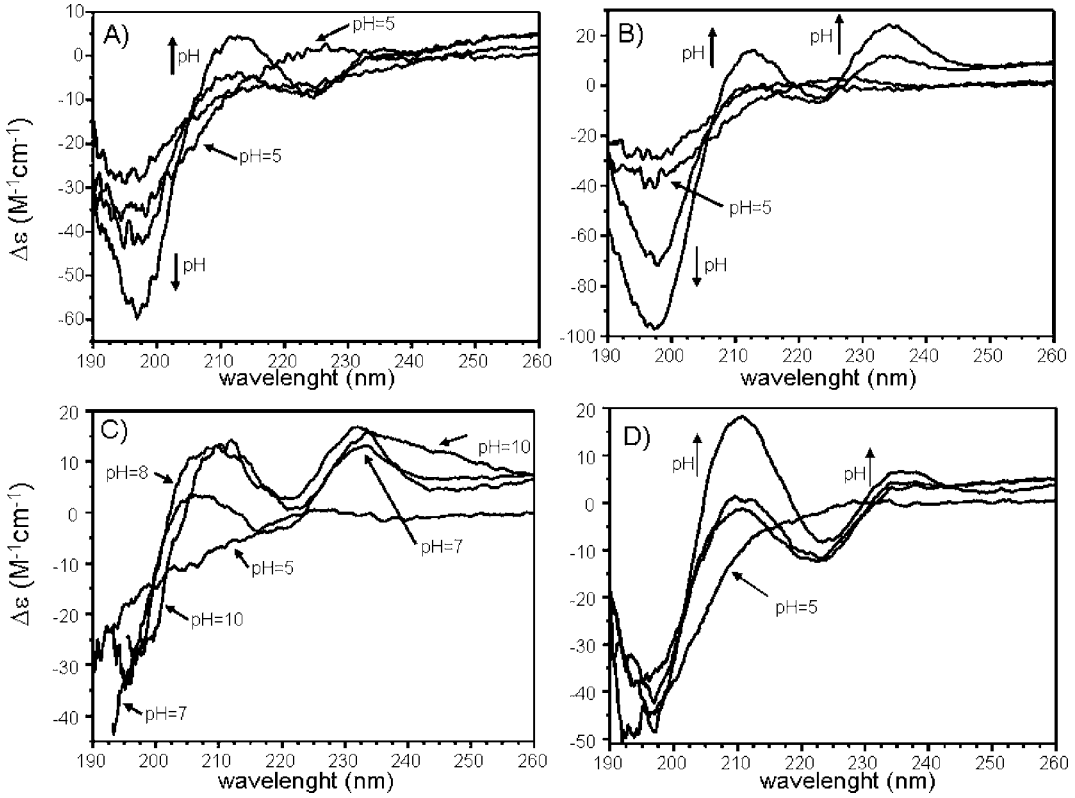

Figure 1. Far-UV CD spectra recorded in H_2O ([L] = 1×10^{-5} M) at different pH values: (A) Cu-hAng(4−17) 1:1 metal to ligand molar ratio; (B) Cu-hAng(4−17) 2:1 metal to ligand molar ratio; (C) Cu-hAng(4−9) 1:1 metal to ligand molar ratio; (D) Cu-hAng(10−17) 1:1 metal to ligand molar ratio.

dx.doi.org/10.1021/ic201300e | *Inorg. Chem.* 2012, 51, 128−141

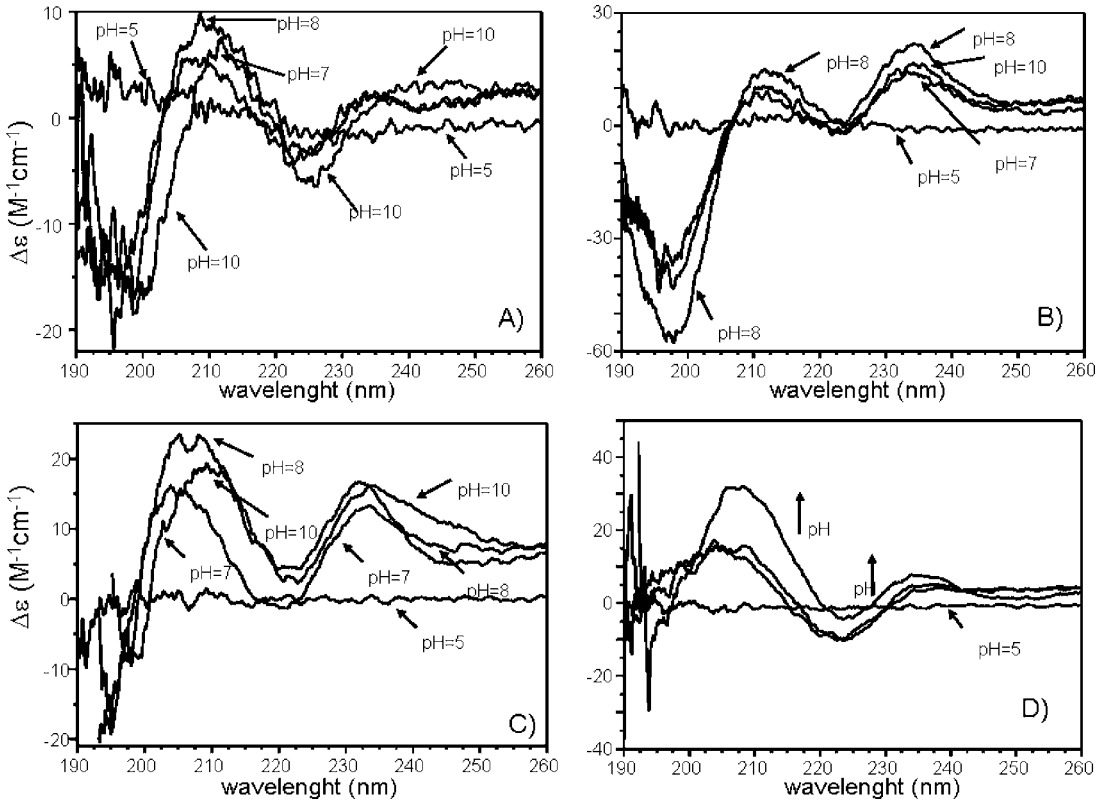

Figure 2. Far-UV CD difference spectra of copper(II) complexes after subtraction of the apo-peptides for Cu- hAng(4−17) at different pH values: (A) Cu-hAng(4−17) (1:1 metal to ligand molar ratio); (B) Cu-hAng(4−17) (2:1 metal to ligand molar ratio); (C) Cu-hAng(4−9) (1:1 metal to ligand molar ratio); (D) Cu-hAng(10−17) (1:1 metal to ligand molar ratio).

also observed at this pH value. The latter band can be assigned to the deprotonated phenolate group of tyrosine residues.[34]

CD spectra of shorter peptide fragments are less influenced by pH variations, especially as regard hAng(10−17). The increase of pH induces a slight decrease of the band intensity at 196−198 nm and at 228 nm. At basic pH the CD spectra of hAng(4−9) show similar features to that of hAng(4−17) with the appearance of a band centered at 245 nm.

Far-UV CD spectra of these copper(II)-peptide systems are reported in Figure 1. The Cu-hAng(4−17) was investigated up to the addition of two equivalent of Cu^{2+}; precipitation phenomena were observed at higher metal concentrations, implying a 2:1 metal to ligand stoichiometry. The Cu-hAng(4−9) and Cu-hAng(10−17) systems were investigated up to one equivalent of metal ion.

The secondary structure of these peptides indisputably changes upon Cu^{2+} addition. The addition of one equivalent of copper(II) to hAng(4−17) induces a decrease of the bands at 196 and 228 nm, up to pH 6 (Figure 1A). The CD difference spectrum, obtained by the subtraction of the parent ligand spectrum, suggests an increase of a turn structure up to pH 6 (Figure 2), determined by copper(II) binding as reported for other linear peptides.[33] Increasing the pH values, a strong increase of the band intensity centered at 196 nm, with a slightly blue-shift at 198 nm, is recorded. Moreover, two bands characterized by a strong maximum at 213 nm and a minimum at 224 nm, together with a weak maximum at 234 nm, are observed. The conformational changes induced by copper addition are similar in the features but more intense than those observed for the parent peptides at basic pH. The spectral features observed, apart from the band at 234 nm, have been assigned to a type II β-turn conformation for linear peptides.[35] Difference spectra give a better perception of the changes induced by the interaction with Cu^{2+} (Figure 2). The increase of pH induces an enhancement of the turn conformation of the peptide resulting from the involvement of backbone amide nitrogen atoms in Cu^{2+} coordination (see next section). The Far-UV CD spectra of Cu(II)-peptide systems are governed by the amide chromophore, but may contain a contribution of aromatic side chains, in particular the band at 234 nm.[36,37] This contribution may change with the induction of a more structured conformation of the peptide. In agreement with the hypothesis of the involvement of aromatic side chains in the CD signals, this band is red-shifted and more broadened at pH 10, as a potential consequence of the phenol deprotonation.[34]

The addition of two equivalents of Cu^{2+} induces more evident secondary structure changes because of metal ion binding (Figure 1B). The difference spectra suggest an increase of the turn structure up to pH 6 as observed after the addition of 1 equivalent of metal ion. In comparison to that observed in the 1:1 system (Figure 2A), a strong increase in the intensity of both the bands at 196 nm and at 211 nm appears upon raising the pH (Figure 2B). Noteworthy, the intensity of the band at 224 nm is reduced and a strong dichroic signal centered at 234 nm appears just at pH 7. In particular, the difference spectra show a strong increase of the band centered at 234 nm, due to the increase of an aromatic contribution to the CD spectra.[36,37]

The addition of one Cu^{2+} equivalent induces different secondary structure changes in the two shorter peptide fragments hAng(4−9) and hAng(10−17) (Figures 1C and 1D). The CD spectra recorded for Cu-hAng(10−17) show strong analogies with spectra obtained for Cu-hAng(4−17) at

dx.doi.org/10.1021/ic201300e | *Inorg. Chem.* 2012, 51, 128−141

1:1 metal to ligand molar ratio. The difference spectra at pH 6 show a strong increase of a turn structure (Figure 2D), while increasing the pH a pattern indicative of type II β-turn conformation, together with a maximum at 234 nm, is observed. Conversely, the CD spectra of Cu-hAng(4−9) show analogies with Cu-hAng(4−17) system at 2:1 metal to ligand molar ratio. In particular, a strong positive band centered at 234 nm starting from pH 7 is observed (Figures 1C and 1D).

The data concerning the copper(II) ions interaction with shorter peptide fragments suggest that the His-13 is more likely the first anchoring site of metal ion for the hAng(4−17) peptide. The strong increase of a positive band at 234 nm observed at 2:1 molar ratio for Cu-hAng(4−17) system indicates a strong structuring effect of the backbone region encompassing His-8, involving a contribution of the Tyr-6 and Phe-9 aromatic side chains.

Speciation, Stability Constants, and Coordination Modes of Cu^{2+} Complexes with hAng(4−17), hAng(4−9), and hAng(10−17). Different ligand to metal molar ratios were used to obtain the stability constants of the metal complexes. The data obtained for mononuclear copper(II) complexes with the short peptides are reported in Table 2 and the distribution diagrams are in Figure 3. The first species formed by hAng(4−9) is $[CuHL]^{2+}$ in which the tyrosine group is still protonated. The stability constant value calculated for this complex species ($\log K = \log \beta_{111} - \log \beta_{011} = 4.13$) is higher than that generally reported for the coordination of only one imidazole nitrogen, suggesting the presence of a backbone carbonyl group in the metal coordination environment in addition to water oxygen atoms as previously found for analogous species.[38,39] This copper(II) complex species forms in a minor amount and its formation is overlapped with that of two other complex species $[CuL]^{+}$ and $[CuH_{-1}L]$, consequently, it was not possible to determine the spectral parameters for the single species. Moreover, up to pH 6, free copper(II) ions are still present as pointed out by the species distribution diagram (Figure 3A) and the EPR spectrum at pH 6 (Figure 4A). The $[CuH_{-1}L]$ species is the prevailing one in

Table 2. Stability Constants ($\log \beta_{pqr}$) and pK Values of Cu (II) Complexes with hAng(4-9) and hAng(10-17) (T = 298 K, I = 0.1 M KNO_3)[a]

	$\log \beta_{pqr}$	
species	hAng(4−9)	hAng(10−17)
CuH_2L		25.86 (3)
CuHL	14.10 (2)	
CuL	7.99 (2)	14.54 (2)
$CuH_{-1}L$	2.41 (1)	5.98 (3)
$CuH_{-1}L_2$	−4.93 (1)	−3.83 (3)
$CuH_{-3}L$	−14.68 (1)	−14.30 (3)
$pK(1/0)$	6.11	
$pK(0/-1)$	5.57	
$pK(-1/-2)$	7.34	8.56
$pK(-2/-3)$	9.75	9.80
pK_{Lys}		10.47

[a]Standard deviations (3σ values) are given in parentheses $pK(n/m)$ values reflect the pK value of copper(II) complexes.

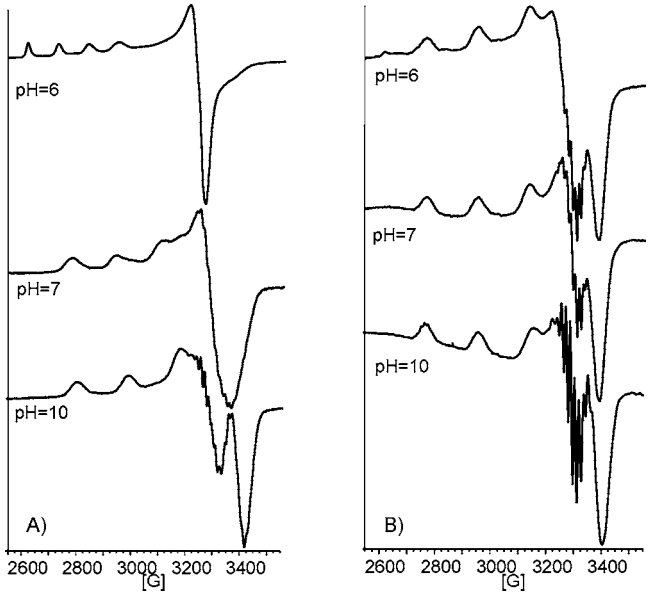

Figure 4. Frozen solution EPR spectra at 150 K at different pH values: (A) Cu-hAng(4−9) system and (B) Cu-hAng(10−17) system. ([Ligand] = $[Cu^{2+}]$ = 1.5 × 10^{-3} M).

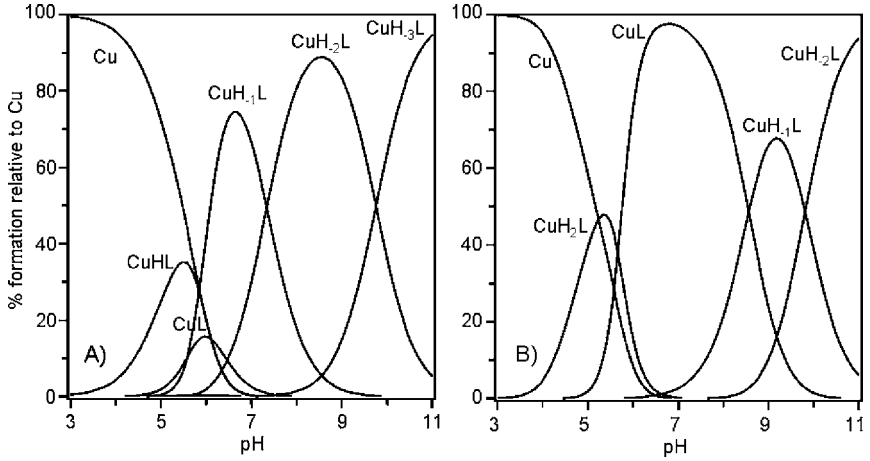

Figure 3. Species distribution diagram for copper(II) complexes with (A) hAng(4−9) and (B) hAng(10−17) ligands. [Ligand] = $[Cu^{2+}]$ = 1.0 × 10^{-3} M.

dx.doi.org/10.1021/ic201300e | Inorg. Chem. 2012, 51, 128−141

Table 3. Spectroscopic Parameters of the Copper(II) Complexes with hAng(4−9) and hAng(10−17)

			UV−vis	CD	EPR	
ligand	pH	species	λ (nm) (ε (M^{-1} cm^{-1}))	λ (nm) ($\Delta\varepsilon$ (M^{-1} cm^{-1}))	$g_{\parallel}$	$A_{\parallel}$ (10^{-4} cm^{-1})
hAng(4−9)	6.5	$CuH_{-1}L$	580(80)	320(0.230); 360(−0.065); 520(0.182); 578(−0.103)	2.230(2)	174(3)
	8.5	$CuH_{-2}L$	523(124)	300(−0.318); 320(0.462); 498(−1.660); 643(1.240)	2.190(1)	193(2)
	10.5	$CuH_{-3}L$	523(130)	299(−0.763); 319(0.269); 499(−1.780); 642(1.264)	2.190(1)	192(2)
hAng(10−17)	5	Cu, CuH_2L	702(50)			
	6−8	CuL	580(91)	297(−0.568); 329(0.650); 490(0.070); 604(−0.600)	2.216(1)	192(2)
	9.2	$CuH_{-1}L$	555(102)	301(0.680); 360(−0.017); 484(0.202); 552(−0.520)	2.208(2)	198(3)
	10.5	$CuH_{-2}L$, $CuH_{-3}L$	555(102)	297(1.180); 352(−0.050); 484(0.200); 552(0.550)	2.208(2)	198(3)

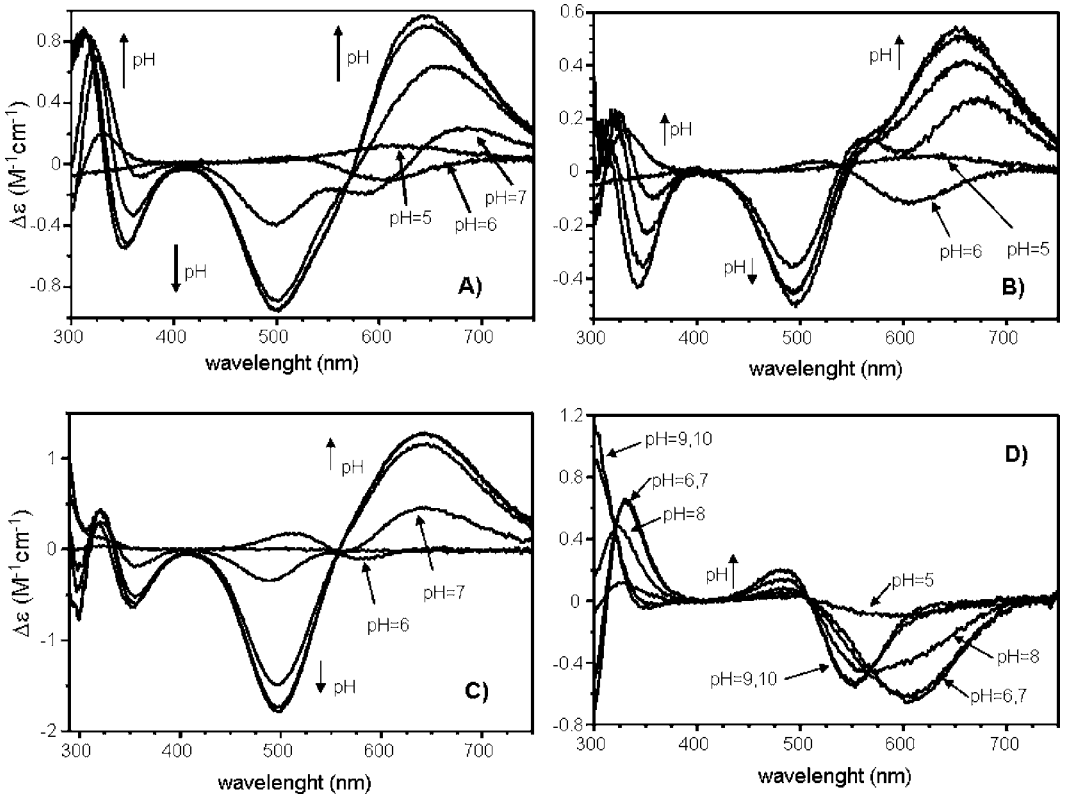

Figure 5. UV−vis CD spectra, at different pH values, of copper(II) complexes with (A) hAng(4−17) 1:1 metal to ligand molar ratio; (B) hAng(4−17) 2:1 metal to ligand molar ratio; (C) hAng(4−9) 1:1 metal to ligand molar ratio; (D) hAng(10−17) 1:1 metal to ligand molar ratio.

the pH range 6−7 and it coexists with $[CuH_{-2}L]^{-}$ in the physiological pH range. The λ_{max} value (Table 3) indicates that $[CuH_{-1}L]$ contains coordinated amide nitrogen atoms. The calculated pK values (Table 2), assigned to amide nitrogen deprotonations from $[CuHL]^{2+}$ to $[CuL]^{+}$ and from $[CuL]^{+}$ to $[CuH_{-1}L]$, are 6.11 and 5.57, respectively. This unusual trend reveals that the deprotonation of the first two amide functions is cooperative.[33] Taking into account that the phenolic group is still not dissociated in this pH range, the real stochiometry of this species is $[CuH_{-2}L(H)]$. The CD spectra confirm the simultaneous presence of the imidazole and the amide nitrogen atoms in the metal coordination environment (Figure 5C) in agreement with EPR parameters that are indicative of a N_{Im},$2N^{-}$ coordination mode. The $[CuH_{-2}L]^{-1}$ is the predominant species increasing the pH value. A marked blue shift of the λ_{max} is observed in agreement with the deprotonation of a third amide nitrogen and the formation of a $[CuH_{-2}L]^{-}$ species containing a N_{Im}, $3N^{-}$ coordination mode, thus the real stoichiometry is $[CuH_{-3}L(H)]^{-}$. The low $g_{\parallel}$ value and the high parallel hyperfine coupling constant value ($A_{\parallel}$) indicate that the metal is coordinated by one imidazole and three nitrogen atoms in an equatorial plane (Table 3). The $[CuH_{-2}L]^{-}$ undergoes further deprotonation to form the $[CuH_{-3}L]^{2-}$ complex species; this species show the same spectroscopic parameters of the previous $[CuH_{-2}L]^{-}$ indicating that the deprotonation step is related to the tyrosine hydroxyl group not involved in the Cu^{2+} binding.

The first species formed by hAng(10−17) is $[CuH_2L]^{2+}$, a metal complex in which the lysine and tyrosine groups are still protonated. The stability constant value calculated for this complex species ($\log K = \log \beta_{121} - \log \beta_{021} = 4.78$) is higher than that reported for the analogous $[CuHL]^{2+}$ species formed by the hAng(4−9) peptide. This is due to the involvement of the imidazole nitrogen and the aspartic carboxylate oxygen atoms in the metal coordination environment, with the formation of a macrochelate ring (Scheme 1).[40−42] The UV−vis absorption data obtained for this copper(II) complex species are similar to those reported for the analogous species with the same coordination environment (Table 3).[40−42] [CuL] starts to form at pH 5 and is the prevailing metal

dx.doi.org/10.1021/ic201300e | Inorg. Chem. 2012, 51, 128−141

Scheme 1. Schematic View of the Copper(II) Complex, $[CuH_2L]$, with hAng(10−17)

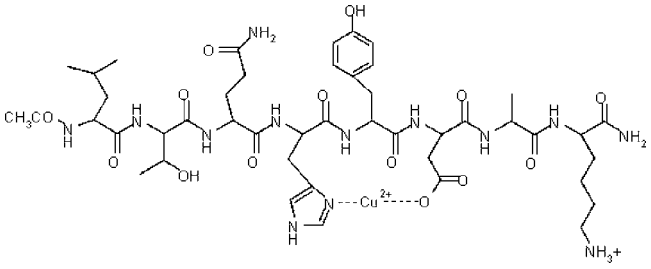

complex species up to pH 8. The spectroscopic parameters show significant changes, due to the involvement of further nitrogen donor atoms in the metal ion coordination environment. The value of λ_{max} at 580 nm and the simultaneous presence of the ligand to metal charge transfer (CT) bands related to amide (297 nm) and imidazole nitrogens (329 nm), indicate the involvement of deprotonated amide and imidazole nitrogen in copper(II) ion binding. At acidic pH, the lysyl ε-amino group is still protonated and the phenolic group is not dissociated so that the real stoichiometry of the species is $[CuH_{-2}L(H_2)]$, with the copper(II) ion bound to one imidazole and two amide nitrogens (N_{Im}, $2N^-$).

The absence of the intermediate species $[CuHL]^+$ is in agreement with that observed for other copper(II)−peptide systems in which the carboxylate is directly involved in metal binding: the macrochelate formation in $[CuH_2L]^{2+}$ delays the formation of the $[CuHL]^+$ species, and the formation of [CuL] takes place in one step, in a cooperative mode.[42−44] A direct contribution by carboxylate in the formation of the [CuL] complex species cannot be ruled out by the potentiometric data. EPR parameters are different from those reported for the analogous complex species [CuL] formed by hAng(4−9) and similar complexes characterized by a N_{Im},$2N^-$ coordination mode.[33,44−48] The $g_{\|}$ and $A_{\|}$ values (Table 3 and Figure 4) indicate the presence of a CuN_3O_1 chromophore in which the nitrogen atoms and the carboxylate oxygen occupy the four equatorial coordination sites, resulting in a higher hyperfine coupling constant value (Table 3 and Figure 4). The UV−vis parameters (Table 3) confirm this planar disposition of the donor atoms bound to the metal ion. It is interesting to note that the high stability constant of [CuL] species formed by hAng(10−17) explains the absence of free copper(II) ions at pH 6.

The $[CuH_{-1}L]^-$ formation is characterized by a blue-shift of UV−vis λ_{max} and an increase of the $N^- \rightarrow Cu(II)$ CT band in the CD spectrum, strongly suggesting the deprotonation of a third amide nitrogen, with a N_{Im}, $3N^-$ coordination mode experienced by Cu^{2+} in the equatorial plane. Also for this complex species, the lysyl ε-amino group is still protonated and the phenolic group is not dissociated, so that the real stoichiometry of the species is $[CuH_{-3}L(H_2)]^-$. The EPR parameters ($g_{\|}$ = 2.208 and $A_{\|}$ = 198 × 10^{-4} cm^{-1}) confirm this coordination mode in which the four nitrogen donor atoms are in a planar arrangement.[44,49] The ε value increases with respect to the previous species suggesting a distorted coordination geometry. Further increase of pH does not affect the spectroscopic parameters, indicating that in the $[CuH_{-2}L]^{2-}$ and $[CuH_{-3}L]^{3-}$ the metal ion has the same coordination environment (N_{Im}, $3N^-$). Indeed, the pK values (Table 4) indicate that this deprotonation processes are associated with

Table 4. Stability Constants (log β) and pK Values of Copper(II) Complexes with hAng(4−17) at 298 K, I = 0.1 M (KNO_3)[a]

species	log β_{pqr} Cu (II)-hAng(4−17)
CuH_4L	40.24(2)
CuH_3L	35.30(1)
CuH_2L	29.10(2)
CuHL	22.74(1)
CuL	14.45(2)
Cu_2HL	27.07(1)
$Cu_2H_{-1}L$	15.14(1)
$Cu_2H_{-2}L$	7.91(2)
$Cu_2H_{-3}L$	−0.56(2)
$Cu_2H_{-4}L$	−9.90(2)
$Cu_2H_{-5}L$	−19.92(2)
$Cu_2H_{-6}L$	−30.13(2)
pK	pK_{pqr} Cu (II)-hAng(4−17)
pK(4/3)	4.94
pK(3/2)	6.19
pK(2/1)	6.36
pK(1/0)	8.27
pK(−1/−2)	7.23
pK(−2/−3)	8.47
pK(−3/−4)	9.34
pK(−4/−5)	10.02
pK(−5/−6)	10.21

[a] 3σ in parentheses pK(n/m) values reflect the pK value of copper(II) complexes.

the phenolic group of tyrosine and amino group of lysine side chains (Tables 1 and 2), taking place at the same pH range values of those pertinent to the free ligand. The absence of spectral changes, also in the visble CD spectra (Figure 5D), indicates that both phenolic and amino group are not directly involved in the copper(II) coordination.

The distribution diagram of the copper(II)-hAng(4−17) system at metal-to-ligand ratio 1:1 is reported in Figure 6A. The metal coordination starts at pH 4 and the first complex species formed, $[CuH_4L]^{3+}$, involves the binding of the imidazole nitrogen of one histidine and the carboxyl group of the aspartate residue (Table 4). In fact, the stability constant value calculated for this complex species (log K = log β_{141} − log β_{041} = 4.30) is higher than that reported for hAng(4−9); this reinforces the indication of the involvement of the carboxylate group, absent in the peptide hAng(4−9). The simple comparison of the log K values may be affected by the different protonation constant values of hAng(4−17), and by the presence of different isomers in which the copper(II) is bound to the aspartic carboxylate oxygen and one imidazole nitrogen atom belonging to His-8 or His-13. Clearly, the formation of a 14-member macrochelate ring involving the carboxylate group of Asp-15 together with the His-13 imidazole side chain is more favored than the 29-member macrochelate ring involving the coordination of the imidazole nitrogen coming from His-8. The UV−vis parameters, determined by spectroscopic titrations (see Experimental Section) for this copper(II) complex species (Table 5) are similar to those reported for the analogous $[CuH_2L]^{2+}$ complex species formed by hAng(10−17), confirming that the copper(II) ion coordination environment involves one imidazole nitrogen atom and a carboxylate group.[40−42]

dx.doi.org/10.1021/ic201300e | Inorg. Chem. 2012, 51, 128−141

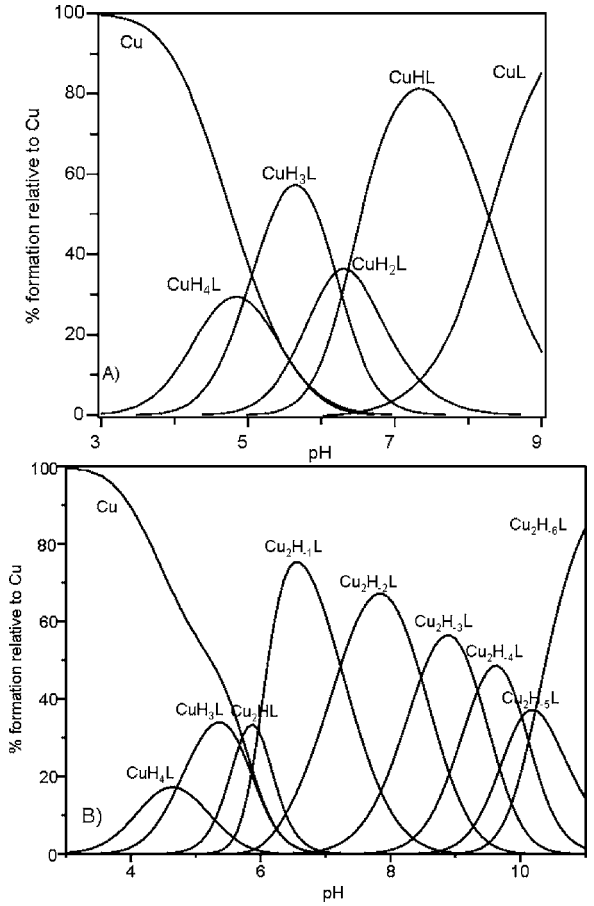

Figure 6. Species distribution diagram of copper(II) complexes with hAng(4−17). [L] = 1 × 10^{-3} M, (A) 1:1 and (B) 2:1 metal to ligand molar ratios).

It is interesting to note that at pH 6 there are no more free copper(II) ions analogously to that reported for the Cu-hAng(10−17) system, a further evidence of the direct involvement of the carboxylate group.

The stability constant value of $[CuH_3L]^{2+}$ (log K = log β_{131} − log β_{031} = 6.13) indicates that the metal ion experiences a macrochelate ring formation with a $2N_{im}$,COO^-_{Asp} coordination environment as reported for other similar peptide fragments.[50] UV−vis CD spectra carried out in the pH range 4−5 (Figure 5A) show low intensity, confirming that the metal ion is coordinated with donor atoms belonging to side chains. The EPR parameters ($g_{\|}$ = 2.296 and $A_{\|}$ = 176 × 10^{-4} cm^{-1}), obtained at pH 5 by subtraction of EPR spectrum recorded at pH 4, and the UV−vis parameters determined by spectroscopic titrations (λ_{max} = 660 nm ε = 58 $M^{-1}cm^{-1}$) are consistent with the presence of a CuN_2O_2 chromophore ($2N_{im}$, COO^-_{Asp}, O_{water}) with the donor atoms arranged in a distorted pseudo-octahedral geometry. Furthermore, this coordination environment is confirmed by the presence of a five-lines superhyperfine structure on the copper fourth line, superimposed to its perpendicular features in the EPR spectrum, indicating the presence of two nitrogen atoms bound to copper (Supporting Information Figure 2S). The $[CuH_2L]^+$ is a minor species and its spectral parameters cannot be determined. The corresponding p*K* value (Table 4) is consistent with the deprotonation of a nitrogen amide atom, while the two tyrosine phenolic groups and the lysine amino group are still protonated, thus the $[CuH_2L]^+$ real stoichiometry is $[CuH_{-1}L(H)]^+$.

The further deprotonation step is associated with a second amide nitrogen atom, so the [CuHL] species corresponds to $[CuH_{-2}L(H_3)]$. The increase of intensity of both the dichroic bands around 360 and 320 nm clearly indicate the simultaneous involvement of the imidazole and amide nitrogens in the copper(II) coordination. It is possible that the copper(II) ion is bound through two imidazole and two amide nitrogens in a plane or one imidazole and two amide nitrogens in a plane with the other imidazole out of the plane as observed for copper(II) complexes with similar peptides encompassing two or three histidine residues.[51−53] The UV−vis parameters (λ = 565 nm and ε = 85 M^{-1} cm^{-1}) indicate the involvement of four nitrogen atom, in an almost planar arrangement. Furthermore, the EPR parameters ($g_{\|}$ = 2.209 and $A_{\|}$ = 198 x10^{-4} cm^{-1}) clearly show an increase of ligand field strength (Figure 7) and, in particular, the high value of the hyperfine constant confirms

Table 5. Spectroscopic Parameters of the Copper(II) Complexes with hAng (4−17) at 1.1 and 2:1 [Cu^{2+}]/Ligand Molar Ratio, Respectively

			UV−vis	CD	EPR	
[Cu^{2+}]/ligand	pH	species	λ (nm) (ε (M^{-1} cm^{-1}))	λ (nm) ($\Delta\varepsilon$ (M^{-1} cm^{-1}))	$g_{\|}$	$A_{\|}$ (10^{-4} cm^{-1})
1:1	4.5	CuH_4L	705(43)			
	5.5	CuH_3L	660(58)	612(0.080)	2.296(2)	176(3)
	6.5	CuH_2L, CuHL		300(−0.307); 327(0.693); 368(−0.080); 500(−0.400); 586(−0.200); 683(0.234)		
	7.5	CuHL	565(85)	322(0.810); 360 (−0.336); 500 (−0.886); 660 (0.640)	2.209(2)	198(3)
	9	CuL	535(107)	314(0.856); 354(−0.511); 500(−0.953); 648(0.900)	2.202(1)	191(3)
2:1	5	Cu, CuH_4L, CuH_3L		309 sh(−0.040); 340 sh(0.017); 353 sh(0.070); 625 (0.060)		
	6	CuH_3L, Cu_2HL, $Cu_2H_{-1}L$	590(90)	302(−0.094); 331(0.150); 522(0.042); 604(−0.115)		
	7	$Cu_2H_{-1}L$, $Cu_2H_{-2}L$	580(155)	302(−0.120); 324(0.220); 359(−0.092); 493(−0.356); 562(0.130); 670(0.265)		
	8	$Cu_2H_{-2}L$	580(190)	321(0.234); 350(−0.232); 497(−0.483); 573 sh(0.114); 660(0.418)		
	9	$Cu_2H_{-3}L$	547(195)	306(0.180); 348(−0.360); 496(−0.450); 564 sh(0.128); 653(0.490)	2.193(1)	185(2)
	10	$Cu_2H_{-4}L$, $Cu_2H_{-5}L$	547(205)	343(−0.418); 495(−0.451); 565 sh(0.093); 650(0.542)	2.193(1)	185(2)
	11	$Cu_2H_{-6}L$	537(230)	343(−0.408); 495(−0.456); 565 sh(0.083); 650(0.550)	2.193(1)	185(2)

dx.doi.org/10.1021/ic201300e | *Inorg. Chem.* 2012, 51, 128−141

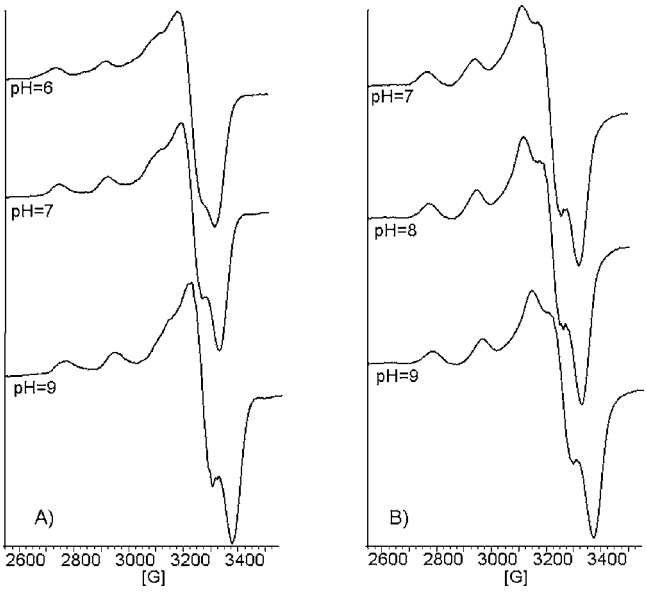

Figure 7. Frozen solution EPR spectra at 150 K at different pH values of Cu-hAng(4−17) system at (A) 1:1 metal to ligand molar ratio and (B) 2:1 metal to ligand molar ratio ([L] = 1.5×10^{-3} M).

the square planar coordination geometry with $2N_{Im},2N^-$ coordination mode, excluding the possibility of a weak interaction of the carboxylate group in an apical position (Scheme 2).

Scheme 2. Schematic View of the Copper(II) Complex, [CuHL], with hAng(4−17)

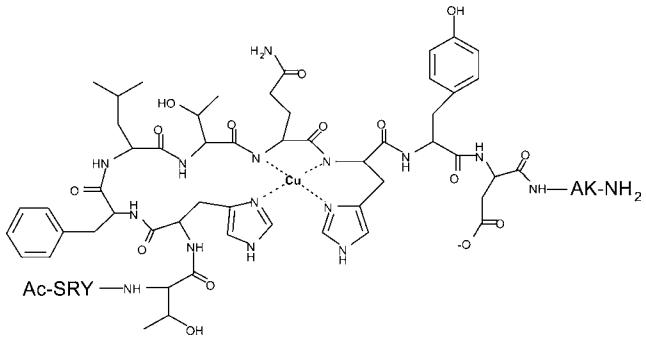

Further deprotonation of an amide nitrogen atom occurs in the species $[CuL]^-$; taking into account the pK values of tyrosine and lysine residues, such a species corresponds to $[CuH_{-3}L(H_3)]^-$, containing a 4N equatorial coordination environment, in which one imidazole nitrogen atom is substituted by an amide group (N_{Im}, $3N^-$). The blue-shift of the λ_{max} and the increase in the molar absorptivity (λ = 535 nm and ε = 107 M^{-1} cm^{-1}) (Table 5) as well as its EPR parameters strengthen this outcome. The slight decrease of the copper hyperfine constant indicates the formation of a more distorted copper coordination polyhedron with a stronger ligand field due to the increased number of amide nitrogen atoms bound to the metal ion in the equatorial plane.

It is interesting to note that the UV−vis CD spectra of the Cu-hAng(4−17) system show some analogies with those obtained for the complexes of the two shorter peptides (Figure 5): up to pH 6 the CD spectrum resembles that of Cu-hAng(10−17); at pH 7 the spectrum appears to be the sum of spectra obtained for copper(II) complexes with hAng(4−9) and hAng(10−17); at basic pH the CD spectra of copper(II) complex species with hAng(4−17) are more similar to those with hAng(4−9) in the d-d transition range, while the bands in the far-UV are more similar to those with hAng(10−17). However, the CD spectra of Cu-hAng(4−17) at 1:1 molar ratio cannot be resolved as the weighted sum of those obtained for Cu-hAng(4−9) and Cu-hAng(10−17) systems: hAng(4−17) forms copper(II) complex species in which both the histidine imidazole side chains are involved in the metal coordination environment; such copper(II) complex species cannot be formed by the shorter peptides.

Differently from the peptides hAng(4−9) and hAng(10−17) that can bind only one copper(II) ion, the peptide hAng(4−17) is able to bind up to two metal ion equivalents (Table 4). The potentiometric results indicate that the mononuclear copper(II) complexes are formed only as minor species at low pH values (Figure 6B). Increasing the pH, only complex species in which the peptide binds two metal ions are observed (Figure 6B and Table 4) and each histidine imidazole nitrogen atom acts as an anchoring site for a single copper(II) ion. The first dinuclear complex species, $[Cu_2HL]^{2+}$, forms around pH 6 and its real stoichiometry is $[Cu_2H_{-2}LH_3]^{2+}$, that contains two deprotonated amide nitrogen atoms. The UV−vis spectra recorded at pH 6 show a broad band centered at 590 nm (Table 5). These features are due to the contemporary presence of different copper(II) complex species and are also indicative of the presence of two copper(II) ions with slightly different coordination environments. The scenario is: one copper(II) ion is bound to one imidazole and one amide nitrogen atom ($1N_{Im}$, $1N^-$) while the second metal ion interacts with one imidazole, one amide and the aspartate carboxylate group. Clearly, in the chromophore CuN_2O_2 ($1N_{Im}$, $1N^-$, $1COO^-_{Asp}$) the His-13 has to be involved in the formation of a more stable macrochelate ring. It is interesting to note that the λ_{max} values determined for the dinuclear $[Cu_2H_{-1}L]$ and $[Cu_2H_{-2}L]$ complexes are very similar to that observed for mononuclear [CuHL] complex, while their molar absorptivities show a significant increase, as expected.

At pH 7 the main complex species is $[Cu_2H_{-1}L]$ that corresponds to $[Cu_2H_{-4}L(H_3)]$, the lysine and the two tyrosine residues being protonated. Each copper(II) ion is coordinated to an imidazole and two deprotonated amide nitrogens ($1N_{Im},2N^-$). The UV−vis bandwidth and the molar absorptivity, calculated by taking into account the metal concentration (ε = 78 M^{-1} cm^{-1}) are very similar to that of the previous species. This indicates that the coordination environment of the copper(II) ion anchored to His-13 still involves the Asp-14 carboxylate group, so that the coordination environments of the two copper(II) ions are different also in this species. The different coordination environments are the cause of the absorption bandwidth. The CD spectra confirm the simultaneous presence of the imidazole and amide nitrogen atoms in the metal coordination sphere, and they appear to be the sum of CD spectra obtained for copper(II) complexes with hAng(4−9) and hAng(10−17) peptides (Figure 5).

The $[Cu_2H_{-2}L]^-$ complex becomes the predominant species at pH 8 and taking into account the pK values of the tyrosine and lysine residues its real stoichiometry can be given as $[Cu_2H_{-5}L(H_3)]^-$. In this species a further amide deprotonation is observed and the two copper(II) ions experience different coordination environments. One Cu^{2+} is bound to one imidazole and two amide ($1N_{Im},2N^-$), while the other metal

dx.doi.org/10.1021/ic201300e | Inorg. Chem. 2012, 51, 128−141

Scheme 3. Schematic View of the Copper(II) Complex, $[Cu_2H_{-3}L]^{2-}$, with hAng(4−17)

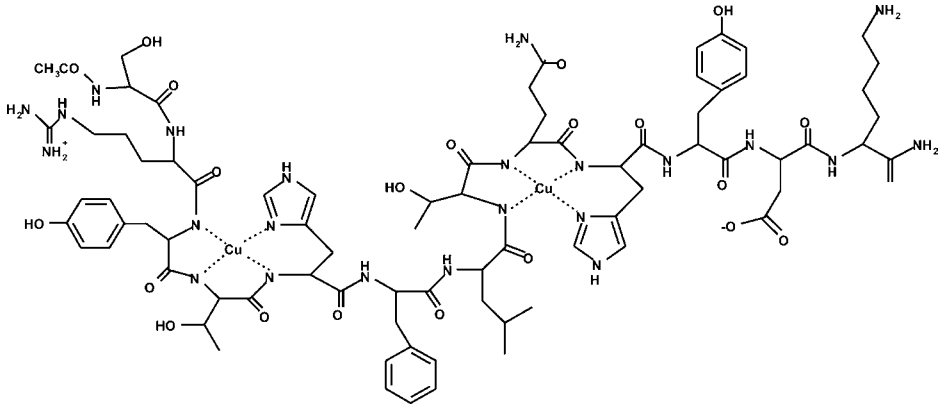

ion is bound to one imidazole and three amide nitrogen atoms ($1N_{Im}$, $3N^-$). These binding details are confirmed by UV−vis band profiles (data not shown) that are the results of the overlap between two distinct bands with maxima at 585 and 545 nm, the latter value associated with the 4N complex species.

Starting from pH 7, the CD spectra show an increase of d-d band intensity, coupled with a decrease of CT bands, in particular of the amide nitrogen atom, in comparison with spectra carried out at 1:1 molar ratio. This is in agreement with the statement that CD spectra of Cu-hAng(4−17) at 2:1, are the combination of the spectra related to the copper(II) complex species formed with the two fragments hAng(4−9) and hAng(10−17) (Figure 5).

The $[Cu_2H_{-3}L]^{2-}$ species forms with a total of six amide donor functions, the real stoichiometry is $[Cu_2H_{-6}L(H_3)]^{2-}$. The visible bandwidth is narrower than that of the previous species, thus indicating that each copper center experiences the same coordination environment ($1N_{Im}$, $3N^-$) (Scheme 3). The complex species $[Cu_2H_{-4}L]^{3-}$, $[Cu_2H_{-5}L]^{4-}$, and $[Cu_2H_{-6}L]^{5-}$ display the same spectroscopic parameters of $[Cu_2H_{-3}L]^{2-}$, indicating that each metal ion experiences the same coordination environment (N_{Im}, $3N^-$). The further deprotonation steps involve tyrosine phenolic groups and lysine ε-amino group, which clearly do not take place in copper(II) ion coordination.

The frozen solution EPR spectra for Cu-hAng(4−17) (2:1 metal to ligand molar ratio) were recorded in the whole pH range investigated. As no antiferromagnetic coupling between the two metal centers was observed, each copper(II) binding site is not influenced by the other. At lower pH, it was not possible to extract the Hamiltonian parameters to the single species owing to the overlap of spectra due to different complex species. Starting from pH 7, the magnetic parameters practically do not change up to pH 10. It is clear that two very similar Cu chromophores were formed and each metal ion is bound to one imidazole and three amide atoms ($1N_{Im}$, $3N^-$) as indicated by potentiometric and spectroscopic results. The parallel hyperfine coupling constant value suggests a departure from the planarity of the copper equatorial coordination plane.

It is relevant to point out that the addition of two equivalents of copper ions results in the presence of a strong dichroic signal at 234 nm starting from pH 7, as evidenced by the CD spectra observed in the range 240−400 nm (Figure 3S). This band is totally absent in the ligand to metal molar ratio 1:1 system and it is present starting from pH 7 in the Cu-hAng(4−9) system but not in the Cu-hAng(10−17). At pH 7 the $[CuH_{-2}L]$ complex species is present in Cu-hAng(4−9) system, in which the copper(II) ion experiences a (N_{Im},$3N^-$) coordination mode. The His-8 is the anchoring site while the deprotonation of the amide nitrogens occurs toward the N-terminus involving the Tyr-6 residue. The CD band at 234 nm can be assigned to this tyrosine side chain group, which changes its position as a consequence of the peptide backbone bending, due to the chelate formation. Also the other His-13 has one closely situated tyrosine residue (Tyr-14), but it is not directly involved in the amide nitrogen deprotonation which occur toward the N-terminus due to the formation of more stable chelate rings.

Copper Complexes with Human Angiogenin Protein. The recombinant hAng was expressed and purified as reported in the Experimental Section. The lack of copper(II) ion bound to the recombinant protein was checked by means of UV−vis spectra (data not shown). The far-UV CD spectra show that the protein secondary structure is β-strands rich. The addition of the copper(II) ion induces a slight decrease of the CD signal (Figure 8).

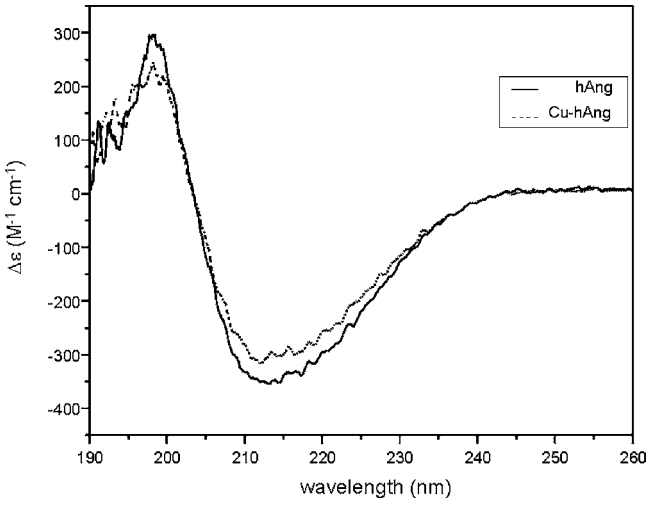

Figure 8. Far-UV CD spectra of hAng protein (10 μM) in MOPS buffer, pH 7.4, continuous line (—) and after the addition of 1 mol equiv of Cu^{2+}, dashed line (---).

The addition of one equivalent of copper(II) to the whole protein at pH 7.4 induces the formation of a band in the visible region, centered at 560 nm, with a molar absorptivity coefficient of 120 M^{-1} cm^{-1}.

dx.doi.org/10.1021/ic201300e | *Inorg. Chem.* 2012, 51, 128−141

The CD spectrum shows the presence of a maximum at 314 nm ($\Delta\varepsilon$ = +0.270) and a minimum at 364 nm ($\Delta\varepsilon$ = −0.034) (Figure 9), and this clearly indicate the contemporary

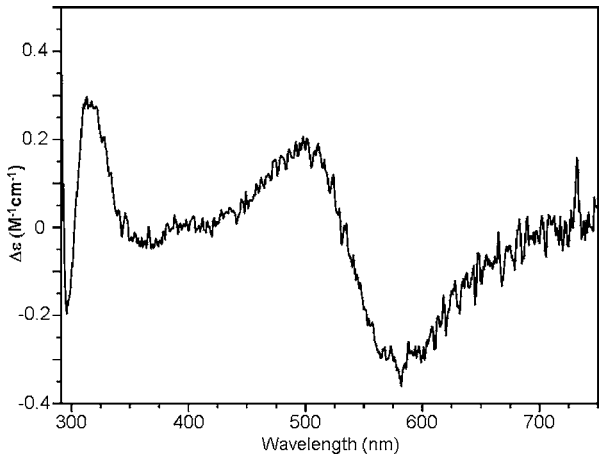

Figure 9. UV−vis CD spectrum at pH 7.4 of Cu-hAng system. [hAng] = [Cu^{2+}] = 5 × 10^{-4} M, in 10 mM MOPS, at pH 7.4.

involvement of imidazole and deprotonated amide nitrogens in the copper(II) binding of the protein. These spectroscopic data strongly suggest the involvement of four nitrogens in the copper(II) coordination environment.

The EPR spectra obtained under the same experimental conditions indicate the presence of a single copper(II) complex species with the following parameters: $g_{\|}$ = 2.202, $A_{\|}$ = 205 × 10^{-4} cm^{-1} (Figure 10). These Hamiltonian values clearly

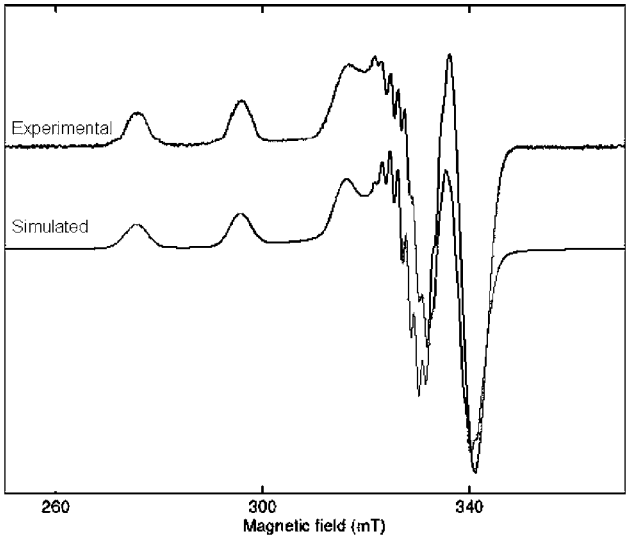

Figure 10. Experimental and simulated EPR spectra of Cu-hAng system. [hAng] = [Cu^{2+}] = 5 × 10^{-4} M, in 10 mM MOPS, at pH 7.4.

indicate the formation of a copper(II) complex species in which the metal ion coordination environment involves four nitrogen atoms. On the basis of Peisach and Blumberg diagrams,[54] the copper(II) ion coordination environment may display 0 or −1 charge, in agreement with the involvement of deprotonated amide nitrogens that neutralize the positive charge of Cu^{2+}.

The human angiogenin encompasses six histidine residues in its sequence and each may represent a potential copper(II) ion anchoring site. The catalytic site for the ribonucleolytic activity of hAng includes the residue His-13, Lys-40, and His-114.[9] Taking into account that the spectroscopic data clearly indicate the involvement of at least one imidazole nitrogen in the Cu^{2+} binding, the RNase catalytic activity of hAng was investigated in the presence of this metal ion to bring into light the involvement of His-13 or His-114 (Figure 11).

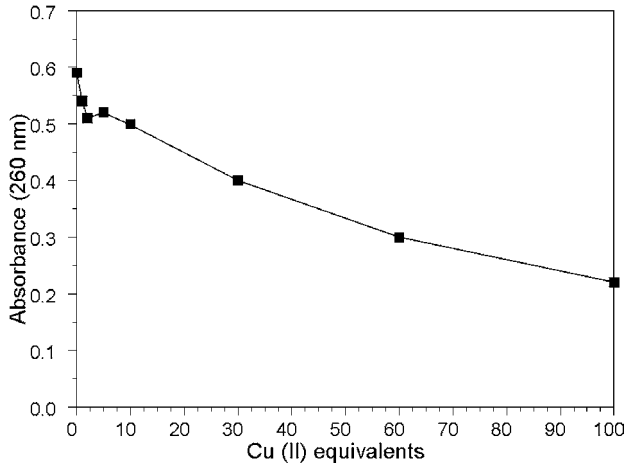

Figure 11. Ribonucleolytic activity of hAng (0.5 μM) after the addition of increasing amount of Cu^{2+}equivalents.

The enzymatic assay was carried out by a modification of Shapiro et al. procedure.[24] In particular, the HEPES buffer,[55] able to bind copper(II) ions,[56] was substituted with MOPS, and the human serum albumin (HSA) was not added to exclude it as a potential copper(II)-binding source. Moreover, all the chemicals were treated with Chelex to minimize the amount of metal ions.

Holloway et al.[22] reported an enzymatic activity of $\Delta A_{260} \approx$ 0.8 at pH 7.0, similar to that we found (~0.6 at pH 7.4). This is in agreement with the bell-shaped pH dependence of the hAng activity previously reported by Lee and Vallee.[55] The maximum activity at pH 6.8 is expected to drop to a value in the range of 65−75% at pH 7.4. A strong decrease of the ribonucleolytic activity was observed at high copper(II)-protein molar ratios (30:1, 100:1). However, a decrease of RNase enzymatic activity was observed just after the addition of one equivalent of Cu^{2+} (Figure 11), suggesting that His-13 and/or His-114 are somehow involved in the metal coordination of hAng.

Preliminary NMR titrations experiments of the ^{15}N labeled hAng with copper(II) ions reveal that the signals of different histidine residues are affected by the metal addition and in particular those related to His-13 and His-65 just adding one copper(II) ion equivalent (data not shown). Thus, Cu^{2+} can "visit" different histidine residues and this should account for the partial decrease of the nuclease activity, lower than that expected in the case of only His-13 or His-114 were involved in the copper(II) ions coordination.

■ CONCLUSIONS

The hAng protein is a potent angiogenic factor and its cellular activities may be affected by copper(II) ions though it is yet unknown how this metal ion is able to produce this effect. Taking into account that copper(II) ion is also an angiogenic factor, a possible metal ion interaction with angiogenin may be part of the mechanisms by which protein functions are regulated in vivo. In this context, the characterization of

dx.doi.org/10.1021/ic201300e | Inorg. Chem. 2012, 51, 128−141

copper(II) complex species with the protein is a valuable mean to understand the potential mutual biological influences. Few studies have been carried out on the interaction between copper and angiogenin, and the identification of the domains involved in metal coordination remains to be determined. It has only been reported that hAng tightly binds about 2.4 copper(II) ions per molecule at physiological pH.[15]

Our preliminary NMR results show that the interaction of Cu^{2+} with ^{15}N labeled hAng, at 1:1 metal to protein molar ratio, affects more than one of the six histidine residues of the recombinant protein. In particular, the NMR signal alteration also involves His-65 and His-13, which are the histidine residues present in the protein domains responsible of protein cell interaction and enzymatic activities, respectively. The ribonucleolytic assay of hAng in the presence of Cu^{2+} again indicates the significant role of His-13 as anchoring site of copper(II) ion.

The comparison of the binding affinity of copper(II) complexes with the peptide fragments encompassing the His-65, previously reported,[17] His-8 and His13 indicates that the peptide containing the His-13 forms the most stable metal complex among the mononuclear species in the physiological pH range.

The peptide hAng(4−17) coordination features show that the two histidine residues act as independent anchoring sites for Cu^{2+}, forming binuclear species in addition to the mononuclear metal complexes. The spectroscopic parameters of the main copper(II) complex with hAng(4−17), [CuHL], are different from those found for the metal ion complex with the recombinant protein, in agreement with the different coordination environment assigned in this work. In particular, our results indicate the involvement of His-8 in the copper(II) binding of hAng(4−17), whereas this does not occur in the whole hAng protein. The UV−vis band features of Cu-hAng system are similar to those obtained for the Cu-hAng(10−17) peptide fragment at pH 7. These data strongly suggest that the His-13 represents one of the preferred copper(II) anchoring site in the whole recombinant protein. His-8 and His-13 are not simultaneously involved in the copper(II) coordination environment, as observed in the [CuHL] species of Cu-hAng(4−17) system. This finding is further confirmed by the differences of the UV−vis CD spectra between Cu-hAng(4−17) and Cu-hAng systems, and by the slight modification of the protein secondary structure recorded upon copper addition. As a matter of fact, the His-13 is located at the end while the His-8 is within the first α-helical region (α-H1, residues 5−13) and the presence of a ($2N_{Im}$, $2N^-$) binding mode with the involvement of His-8 and His-13 should produce a larger change in the protein secondary structure. The EPR parameters obtained for Cu-hAng system are indicative of the presence of four nitrogens in a planar disposition in the copper(II) ions coordination environment with a stronger equatorial field than that observed for [CuHL] species of Cu-hAng(4−17). We can speculate that the differences with the magnetic parameters of the hAng(10−17) can be attributed to the hydrogen bond network around the His13 in the protein that can favor the deprotonation of amide nitrogen giving rise to a N_{Im}, $3N^-$ coordination mode that is partly present in the peptide fragment at physiological pH value.

It is interesting to highlight that the presence of deprotonated amide nitrogen atoms in the copper(II) ions coordination within a protein is only observed for such proteins as prion (PrP^C) which display a high affinity for the copper ions.[57]

The high affinity for copper ions showed by the hAng protein may explain their potential interactions in vivo, and then of a possible direct correlation between copper and angiogenin. In this context, further studies by means of NMR and ESI-MS are currently in progress to better elucidate the metal−protein loading ability, the related binding site/sites of the protein and the possible competition with other copper(II) binding molecules in vivo.

■ ASSOCIATED CONTENT

Supporting Information

Addtional figures. This material is available free of charge via the Internet at http://pubs.acs.org.

■ AUTHOR INFORMATION

Corresponding Author

*Phone: +39 095 7385070. Fax: +39 095 337678. E-mail: erizzarelli@unict.it.

Present Addresses

[‖]Istituto di Biostrutture e Bioimmagini - CNR - Catania, Viale A. Doria 6, 95125 Catania, Italy.

[⊥]Scuola Superiore di Catania, Via Valdisavoia 9, 95123 Catania, Italy.

■ ACKNOWLEDGMENTS

This work was supported by MIUR, FIRB RBNE08HWLZ001. E.R. and D.L.M. wish to thank the Short Term Mobility Program of National Council of Research (CNR-Rome). Authors thank Prof. R.P. Bonomo for helpful discussion and Tiziana Campagna and Gaetano Strano for technical assistance.

■ REFERENCES

(1) Fett, J. W.; Strydom, D. J.; Lobb, R. R.; Alderman, E. M.; Bethune, J. L.; Riordan, J. F.; Vallee, B. L. *Biochemistry* **1985**, *24*, 5480−5486.

(2) Strydom, D. J.; Fett, J. W.; Lobb, R. R.; Alderman, E. M.; Bethune, J. L.; Riordan, J. F.; Vallee, B. L. *Biochemistry* **1985**, *24*, 5486−5494.

(3) Kurachi, K.; Davie, E. W; Strydom, D. J.; Vallee, B. L. *Biochemistry* **1985**, *24*, 5494−5499.

(4) Soncin, F.; Shapiro, R.; Fett, J. W. *J. Biol. Chem.* **1994**, *269*, 8999−9005.

(5) Kishimoto, K.; Liu, S.; Tsuji, T.; Olson, A. K.; Hu, G. F. *Oncogene* **2005**, *24*, 445−456.

(6) Folkman, J.; D'Amore, P. A. *Cell* **1996**, *87*, 1153−1155.

(7) Tello-Montoliu, A.; Patel, J. V.; Lip, G. Y. *J. Thromb. Haemost.* **2006**, *4*, 1864−1874.

(8) Vallee, B. L.; Riordan, J. F. *Cell. Mol. Life Sci.* **1997**, *53*, 803−815.

(9) Strydom, D. J. *Cell. Mol. Life Sci.* **1998**, *54*, 811−824.

(10) Badet, J.; Soncin, F.; Guitton, J. D.; Lamare, O.; Cartwright, T.; Barritault, D. *Proc. Natl. Acad. Sci. U. S. A.* **1989**, *86*, 8427−8431.

(11) Kaplan, J. H.; Lutsenko, S. *J. Biol. Chem.* **2009**, *284*, 25461−25465.

(12) Lowndes, S. A.; Harris, A. L. *J. Mammary Gland Biol. Neoplasms* **2005**, *10*, 299−310.

(13) Goodman, V. L.; Brewer, G. J.; Merajver, S. D. *Curr. Cancer Drug Targets* **2005**, *5*, 543−549.

(14) Finney, L.; Mandava, S.; Ursos, L.; Zhang, W.; Rodi, D.; Vogt, S.; Legnini, D.; Maser, J.; Ikpatt, F.; Olopade, O. I.; Glesne, D. *Proc. Natl. Acad. Sci. U. S. A.* **2007**, *104*, 2247−2252.

(15) Soncin, F.; Guitton, J. D.; Cartwright, T.; Badet, J. *Biochem. Biophys. Res. Commun.* **1997**, *236*, 604−610.

(16) Hu, G. F. *J. Cell. Biochem.* **1998**, *69*, 326−335.

(17) La Mendola, D.; Magrì, A.; Vagliasindi, L. I.; Hansson, Ö.; Bonomo, R. P.; Rizzarelli, E. *Dalton Trans.* **2010**, 10678−10684.
(18) Acharya, K. R.; Shapiro, R.; Allen, S. C.; Riordan, J. F.; Vallee, B. L. *Proc. Natl. Acad. Sci. U. S. A.* **1994**, *91*, 2915−2919.
(19) Papageorgiou, A. C.; Shapiro, R.; Acharya, K. R. *EMBO J.* **1997**, *16*, 5162−5177.
(20) Lequin, O.; Thuering, H.; Robin, M.; Lallemand, J. Y. *Eur. J. Biochem.* **1997**, *250*, 712−726.
(21) La Mendola, D.; Bonomo, R. P.; Caminati, S.; Di Natale, G.; Emmi, S. S.; Hansson, Ö.; Maccarrone, G.; Pappalardo, G.; Pietropaolo, A.; Rizzarelli, E. *J. Inorg. Biochem.* **2009**, *103*, 195−204.
(22) Holloway, D. E.; Hares, M. C.; Shapiro, R.; Subramanian, V.; Acharya, K. R. *Protein Expr. Purif.* **2001**, *22*, 307−317.
(23) Jang, S. H.; Kang, D. K.; Chang, S. I.; Scheraga, H. A.; Shin, H. C. *Biotechnol. Lett.* **2004**, *26*, 1501−1504.
(24) Shapiro, R.; Weremowicz, S.; Riordan, J. F.; Vallee, B. L. *Proc. Natl. Acad. Sci. U. S. A.* **1987**, *84*, 8783−8787.
(25) Bonomo, R. P.; Bruno, V.; Conte, E.; De Guidi, G.; La Mendola, D.; Maccarrone, G.; Nicoletti, F.; Rizzarelli, E.; Sortino, S.; Vecchio, G. *Dalton Trans.* **2003**, 4406−4415.
(26) Gans, P.; Sabatini, A.; Vacca, A. *Talanta* **1996**, *43*, 1739−1753.
(27) Alderighi, L.; Gans, P.; Ienco, A.; Peters, D.; Sabatini, A.; Vacca, A. *Coord. Chem. Rev.* **1999**, *184*, 311−318.
(28) Stoll, S.; Schweiger, A. *J. Magn. Reson.* **2006**, *178*, 42−55.
(29) Kallay, C.; Varnagy, K.; Micera, G.; Sanna, D.; Sovago, I. *J. Inorg. Biochem.* **2005**, *99*, 1514−1525.
(30) Kowalik- Jankowska, T.; Jankowska, E.; Kasrzykowski, F. *Inorg. Chem.* **2010**, *49*, 2182−2192.
(31) Kulon, K.; Valensin, D.; Kamysz, W.; Valensin, G.; Nadolski, P.; Porciatti, E.; Gaggelli, E.; Kozlowski, H. *J. Inorg. Biochem.* **2008**, *102*, 960−972.
(32) Sanna, D.; Micera, G.; Kallay, C.; Rigo, V.; Sovago, I. *Dalton Trans.* **2004**, 2702−2707.
(33) Di Natale, G.; Grasso, G.; Impellizzeri, G.; La Mendola, D.; Micera, G.; Mihala, N.; Nagy, Z.; Osz, K.; Pappalardo, G.; Rigo, V.; Rizzarelli, E.; Sanna, D.; Sovago, I. *Inorg. Chem.* **2005**, *44*, 7214−7225.
(34) Pietropaolo, A.; Muccioli, L.; Zannoni, C.; La Mendola, D.; Maccarrone, G.; Pappalardo, G.; Rizzarelli, E. *J. Phys. Chem. B* **2008**, *112*, 5182−5188.
(35) Perczel, A.; Hollosi, M. In *Circular Dichroism and the Conformational Analysis of Biomolecules*; Fasman, G. D., Ed.; Plenum Press: New York, 1996, pp 285−380.
(36) Krittinai, C.; Johnson, W. C. *Anal. Biochem.* **1997**, *253*, 57−64.
(37) Chakrabartty, A.; Kortemme, T.; Padmanabhan, S.; Baldwin, R. L. *Biochemistry* **1993**, *32*, 5560−5565.
(38) La Mendola, D.; Bonomo, R. P.; Impellizzeri, G.; Maccarrone, G.; Pappalardo, G.; Rizzarelli, E.; Pietropaolo, A.; Zito, V. *J. Biol. Inorg. Chem.* **2005**, *10*, 463−475.
(39) Orfei, M.; Alcaro, M. C.; Chelli, G. M. M.; Gianneschi, M.; Kozlowki, H.; Brasun, J.; Messori, L. *J. Inorg. Biochem.* **2003**, *97*, 299−307.
(40) Boka, B.; Myari, A.; Sovago, I.; Hadjliadis, N. *J. Inorg. Biochem.* **2004**, *98*, 113−122.
(41) Karavelas, T.; Malandrinos, G.; Hadjiliadis, N.; Mlynarz, P.; Kozlowski, H.; Barsan, M.; Butler, I. *Dalton Trans.* **2008**, 1215−1223.
(42) La Mendola, D.; Magrì, A.; Hansson, Ö; Bonomo, R. P.; Rizzarelli, E. *J. Inorg. Biochem.* **2009**, *103*, 758−765.
(43) Kallay, C.; Varnagy, K.; Micera, G.; Sanna, D.; Sovago, I. *J. Inorg. Biochem.* **2005**, *99*, 1514−1525.
(44) La Mendola, D.; Magrì, M.; Campagna, T.; Campitiello, M. A.; Raiola, L.; Isernia, C.; Hansson, Ö.; Bonomo, R. P.; Rizzarelli, E. *Chem.—Eur. J.* **2010**, *16*, 76212−6223.
(45) Kowalik-Jankowska, T.; Ruta-Dolejsz, M.; Wisniewska, K.; Lankiewicz, L.; Kozlowski, H. *J. Chem. Soc., Dalton Trans.* **2000**, 4511−4519.
(46) Zoroddu, M. A.; Kowalik-Jankowska, T.; Medici, S.; Peana, M.; Kozlowski, H. *Dalton Trans.* **2008**, 6127−6134.
(47) Varnagy, K.; Boka, B.; Sovago, I.; Sanna, D.; Marras, P.; Micera, G. *Inorg. Chim. Acta* **1998**, *275*−*276*, 440−446.
(48) Rivillas-Acevedo, L.; Grande-Aztatzi, R.; Lomelì, I.; Garcia, J. E.; Barrios, E.; Teloxa, S.; Vela, A.; Quintanar, L. *Inorg. Chem.* **2011**, *50*, 1956−1972.
(49) Mylonas, M.; Plakatouras, J. C.; Hadjiliadis, N.; Krezel, A.; Bal, W. *Inorg. Chim. Acta* **2002**, *339*, 60−70.
(50) Travaglia, A.; Arena, G.; Fattorusso, R.; Isernia, C.; La Mendola, D.; Malgieri, G.; Nicoletti, V. G.; Rizzarelli, E. *Chem.—Eur. J.* **2011**, *17*, 3726−3738.
(51) Casolaro, M.; Chelli, M.; Ginanneschi, M.; Laschi, F.; Messori, L.; Muniz-Mirand, M.; Papini, A. M.; Kowalik-Jankowska, T.; Kozlowski, H. *J. Inorg. Biochem.* **2002**, *89*, 181−190.
(52) Jancso, A.; Paksi, Z.; Jakab, N.; Gyurcsik, B.; Rockenbauer, A.; Gajda, T. *Dalton Trans.* **2005**, 3187−3194.
(53) Kallay, C.; Varnagy, K.; Malandrinos, G.; Hadjiliadis, N.; Sanna, D.; Sovago, I. *Dalton Trans.* **2006**, 4545−4552.
(54) Peisach, J.; Blumberg, W. E. *Arch. Biochem. Biophys.* **1974**, *165*, 691−708.
(55) Lee, F. S.; Vallee, B. L. *Biochem. Biophys. Res. Commun.* **1989**, *161*, 121−126.
(56) Sokolowska, M.; Bal, W. *J. Inorg. Biochem.* **2005**, *99*, 1653−1660.
(57) Millhauser, G. L. *Annu. Rev. Phys. Chem.* **2007**, *58*, 299−320.